catalysts

MDPI

Article

New Ni(II)-Ni(II) Dinuclear Complex, a Resting State of the (α-diimine)$NiBr_2$/$AlMe_3$ Catalyst System for Ethylene Polymerization

Igor E. Soshnikov [1,*], Nina V. Semikolenova [1], Anna A. Bryliakova [1,2], Artem A. Antonov [1], Konstantin P. Bryliakov [1] and Evgenii P. Talsi [1,*]

[1] Boreskov Institute of Catalysis, Pr. Lavrentieva 5, 630090 Novosibirsk, Russia
[2] Department of Natural Sciences, Novosibirsk State University, Pirogova 1, 630090 Novosibirsk, Russia
* Correspondence: soshnikov@catalysis.ru (I.E.S.); talsi@catalysis.ru (E.P.T.)

Abstract: A novel room-temperature stable diamagnetic nickel complex **2** was detected upon activation of Brookhart-type ethylene polymerization pre-catalyst $LNiBr_2$ (**1**, L = 1,4-bis-2,4,6-trimethylphenyl-2,3-dimethyl-1,4-diazabuta-1,3-diene) with $AlMe_3$. Using in situ ^1H, ^2H, and ^{13}C NMR spectroscopy, as well as DFT calculations, this species has been identified as an antiferromagnetically coupled homodinuclear complex $[LNi^{II}(\mu\text{-}Me)(\mu\text{-}CH_2)Ni^{II}L]^+Br^-$. Its behavior in the reaction solution is characteristic of the resting state of nickel catalyzed ethylene polymerization.

Keywords: α-diimine; nickel; trimethylaluminum; NMR; ethylene polymerization; active species; DFT calculations

check for updates

Citation: Soshnikov, I.E.; Semikolenova, N.V.; Bryliakova, A.A.; Antonov, A.A.; Bryliakov, K.P.; Talsi, E.P. New Ni(II)-Ni(II) Dinuclear Complex, a Resting State of the (α-diimine)$NiBr_2$/$AlMe_3$ Catalyst System for Ethylene Polymerization. *Catalysts* **2023**, *13*, 333. https://doi.org/10.3390/catal13020333

Academic Editors: Maria Jaworska and Piotr Lodowski

Received: 19 December 2022
Revised: 28 January 2023
Accepted: 31 January 2023
Published: 2 February 2023

1. Introduction

During the first two decades of the 21st century, Ni(II) α-diimines have remained the subject of extensive studies due to their unique ability to catalyze the formation of branched polyethylene from ethylene as the sole feedstock, as well as copolymerization of ethylene with polar monomers [1–28]. Despite a great number of publications devoted to their mechanistic investigations [29–56], some crucial details of the catalytic process remained unclear. For example, some data on the nature of the active species formed upon activation of α-diimine Ni(II) complexes with MAO and MMAO have been obtained. Namely, cationic Ni(II)-alkyl species—direct precursors of the ethylene polymerization active sites [29,30]—were detected in situ by NMR in the real catalyst systems $LNiBr_2$/MAO and $LNiBr_2$/MMAO [46].

In contrast, the nature of the Ni(II) complexes formed upon activation of $LNiBr_2$ with $AlMe_3$ have not yet been reported. Meanwhile, there have been several examples of using trimethylaluminum alone as an effective co-catalyst for Ni(II) α-diimines [25,34,51,54–57].

Recently, we reported the detection and characterization of a paramagnetic monovalent nickel complex $[LNi^{I}(\mu\text{-}Me)_2AlMe_2]$ formed upon activation of complex **1** (Figure 1) with $AlMe_3$ [51,53,56]. Herein, we report formation of novel diamagnetic nickel(II) species in this system in the presence of a small excess of $AlMe_3$ (Al/Ni = 10). The new species have been characterized in detail by in situ ^1H, ^2H, and ^{13}C NMR spectroscopy, and their assignment has been corroborated by quantum chemical (DFT) calculations.

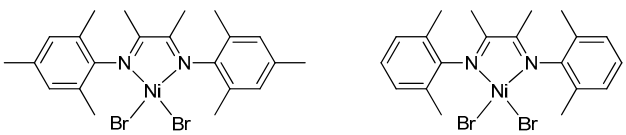

Figure 1. Complexes **1** and **1′** studied herein.

2. Results and Discussion

2.1. The Nickel Center Spin State

It is well-known that a Ni(II) center ($3d^8$ configuration) can exist in two spin states: paramagnetic high-spin ($S = 1$) and diamagnetic low-spin ($S = 0$). As a rule, four-coordinated Ni(II) complexes with square–planar geometry are diamagnetic, whereas distorted tetrahedral counterparts are paramagnetic (see, for example, Refs. [58–61]). The low-spin Ni(II) species display well-resolved ^{1}H NMR resonances in the range typical for diamagnetic species. On the contrary, the high-spin Ni(II) complexes display broad and paramagnetically shifted ^{1}H NMR peaks [62]. The paramagnetic shifts are temperature-dependent, obeying the Curie's law (inverse proportionality with temperature). In addition, the high-spin Ni(II) species are EPR-silent in the X-band due to high zero-field splitting ($D >> h\nu$) [63].

Complexes of Ni(I) ($3d^9$ configuration) are paramagnetic ($S = 1/2$) and usually display well-resolved X-band EPR resonances at $g > g_e$ due to the negative spin-orbit coupling constant. Typically, for such species, only very broad ^{1}H NMR resonances can be detected.

Diamagnetism of nickel(I) species can also be the case due to antiferromagnetic coupling of two paramagnetic centers ($S_1 = S_2 = 1/2$; $S_\Sigma = S_1 + S_2 = 0$ ground state); some diamagnetic dinuclear Ni^I-Ni^I complexes have been reported [64]. Besides, diamagnetic state can be realized for Ni(I) complexes with α-diimine anion-radical ($L^{(\cdot-)}$) as a ligand. In this case, antiferromagnetic coupling between the Ni(I) center ($S = 1/2$) and anion-radical ($L^{(\cdot-)}$) ($S = 1/2$) results in zero overall spin. In the latter two cases, the temperature dependence of the paramagnetic shifts of the ^{1}H NMR resonances does not obey Curie's law; these shifts increase with temperature in line with the growing population of the paramagnetic excited state ($S = 1$).

Complex **2,** reported herein, can be obtained via the reaction of **1** with a relatively small excess of $AlMe_3$ (10 equiv.) in toluene at room temperature. Note that **2** displays good thermal stability at room temperature and rapidly decomposes only at $T > 40$ °C. Nevertheless, our numerous attempts to isolate **2** from the solution for its X-ray structural characterization have remained unsuccessful. Fortunately, **2** had rather informative ^{1,2}H and ^{13}C NMR spectra.

The ^{1}H NMR spectra of **2** recorded at different temperatures are shown in Figure 2. The resonances of **2** are spread over a range of 8 . . . −1.5 ppm, which is typical for diamagnetic species, their chemical shifts demonstrating very weak temperature dependence. It is worth noting that some resonances of **2** in the range of 6.4 . . . 6.8 and 1.6 . . . 2.3 ppm, marked by asterisks, coalesce at 40 °C. The reason for such behavior will be discussed below.

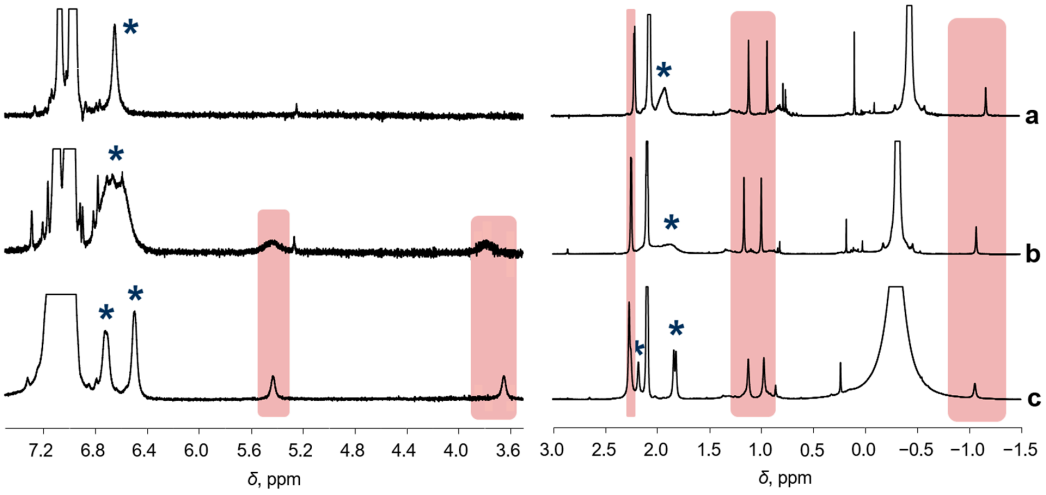

Figure 2. The ^{1}H NMR spectra (toluene-d_8, [Al]/[Ni] = 10/1, C_{Ni} = 5 mM) of the sample **1**/$AlMe_3$, recorded at different temperatures: 40 °C (**a**), 25 °C (**b**), and −20 °C (**c**). Asterisks mark the resonances that coalesce at 40 °C. Other resonances of **2** are highlighted.

2.2. The ^{1}H NMR Resonances of the α-Diimine Ligand of **2**

The ^{1}H NMR spectrum of the sample **1**/$AlMe_3$ (toluene-d_8, [Al]/[Ni] = 10/1, C_{Ni} = 5 mM) recorded at 0 °C displays narrow well-resolved resonances of the α-diimine protons of the ligand of **2** (Figure 3a).

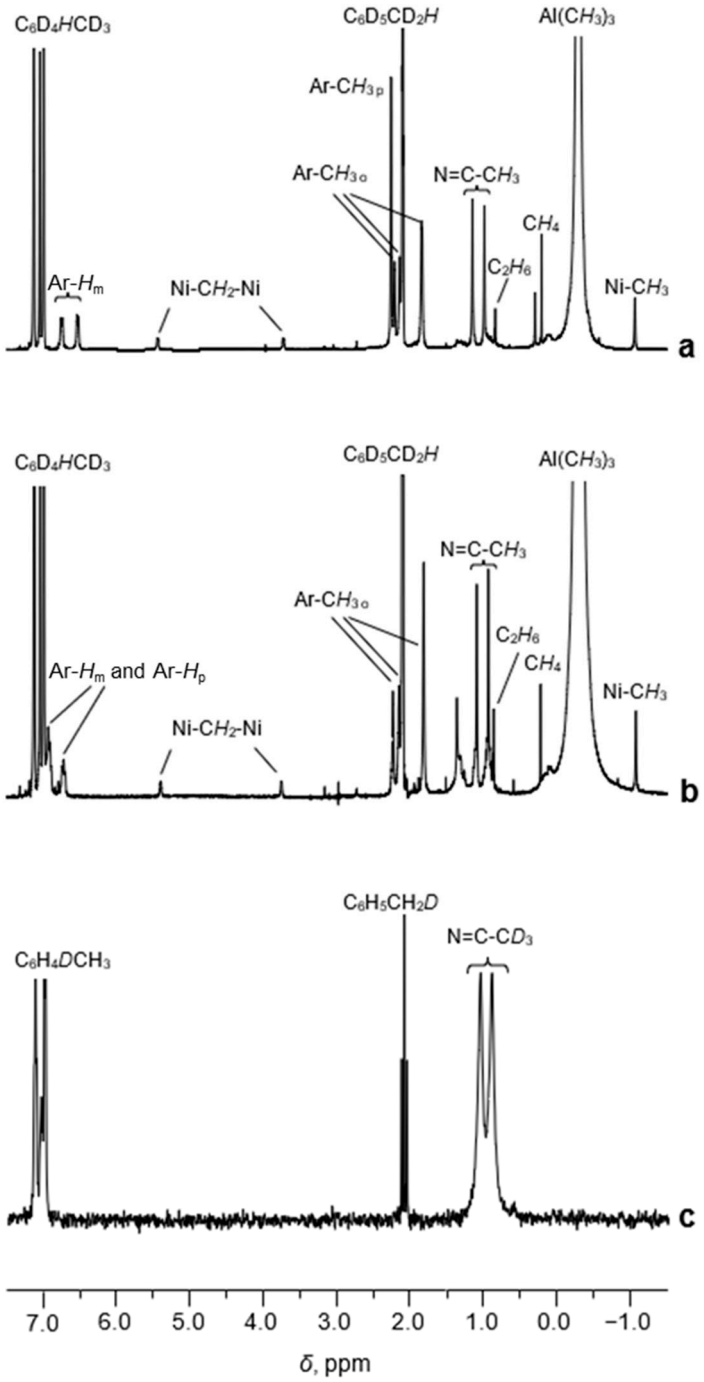

Figure 3. The ^{1}H NMR spectra (toluene-d_8, [Al]/[Ni] = 10/1, C_{Ni} = 5 mM, 0 °C) of the samples **1**/$AlMe_3$ (**a**) and **1′**/$AlMe_3$ (**b**). The ^{2}H NMR spectrum of the sample $\mathbf{1^D}$/$AlMe_3$ (toluene, [Al]/[Ni] = 10/1, C_{Ni} = 5 mM) recorded at 0 °C (**c**).

A singlet at δ 2.27 corresponds to *para*-Me-substituents at the aromatic rings of **2**. Indeed, the ^{1}H NMR spectrum of the sample **1′**/$AlMe_3$ (α-diimine ligand of **1′** contains no *para*-methyl substituents, Figure 1) displays no such resonance (Figure 3b). Two singlets at δ 0.98 and δ 1.14 are assigned to the methyl protons of the CH_3-C=N moieties. To corroborate

this assignment, the ^{2}H NMR spectrum of the sample $\mathbf{1^D}$/$AlMe_3$ was recorded (toluene, [Al]/[Ni] = 10/1, C_{Ni} = 5 mM, $\mathbf{1^D}$—complex **1**, selectively enriched (ca. 86%) by ^{2}H isotope in the *Me*-C=N moiety). The corresponding ^{2}H resonances of the CD_3-C=N groups are observed at δ 0.90 and δ 1.05, respectively (Figure 3c), witnessing a small isotopic shift compared to the ^{1}H peaks of the non-labeled prototype.

The resonances in the range 6.5−6.8 ppm belong to the aromatic protons of the α-diimine ligand, whereas four broadened singlets at 2.21, 2.14, 1.83, and 1.82 ppm can be assigned to the *o*-Me protons (Figure 3a). The integral intensities of these resonances are in agreement with our assignment (Table S1, SM).

Besides the resonances of the α-diimine ligand, the ^{1}H NMR spectrum of **1**/$AlMe_3$ (Figures 3a and 4a) displays three additional signals at δ 5.44 (br d, $^2J_{HH}$ = 3.5 Hz), δ 3.72 (br. d, $^2J_{HH}$ = 3.5 Hz), and δ −1.07 (s). The last one is characteristic of the protons of Me-group, directly bonded to the Ni(II) center (see, for example, Ref. [28]). This assignment was confirmed by ^{13}C and ^{1}H NMR (Figures 4 and 5) of the sample **1**/$AlMe_3$* containing ^{13}C-enriched (ca. 54 at.%) trimethylaluminum and ^{1}H-^{13}C hxdeptbiqf NMR of **1**/$AlMe_3$ one (Figure S2). The ^{1}H NMR spectrum of **1**/$AlMe_3$* displayed a doublet at δ −1.07 with $^1J_{CH}$ = 125.2 Hz (Figure 4a,b), with the corresponding singlet at in dept135 ^{13}C NMR being found at δ −25.2 (Figure 5). The corresponding cross-peak in ^{1}H-^{13}C NMR was also observed (Figure S2 in SM). The integral intensity of ^{1}H NMR resonance at δ −1.07 indicates that the molecule of **2** contains two α-diimine ligands per Ni-*Me* group.

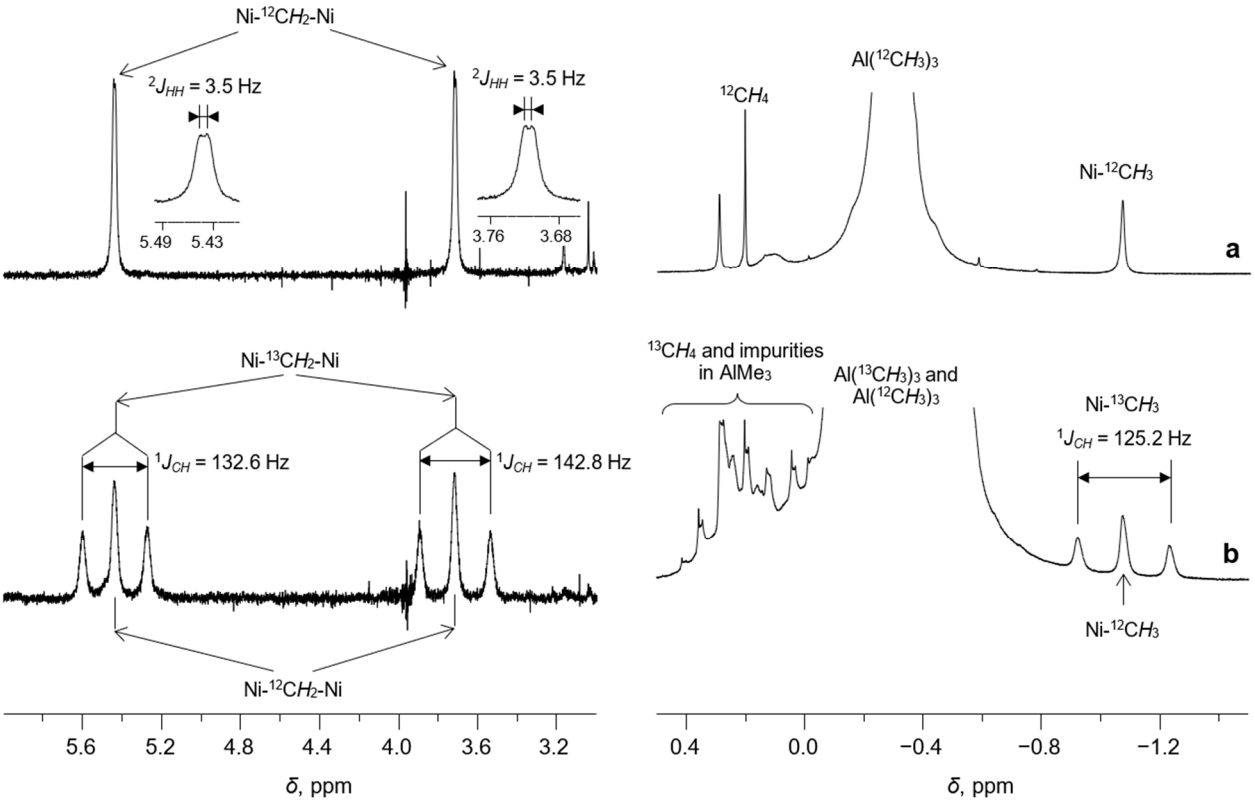

Figure 4. Expanded regions (6.0 … 3.0 and 0.5 … −1.5 ppm) of the ^{1}H NMR spectra (toluene-d_8, [Al]/[Ni] = 10/1, C_{Ni} = 5 mM, 0 °C) of the samples **1**/$AlMe_3$ (**a**) and **1**/$AlMe_3$* (**b**). $AlMe_3$* is a trimethylaluminum enriched by ^{13}C isotope (ca. 54 at.%).

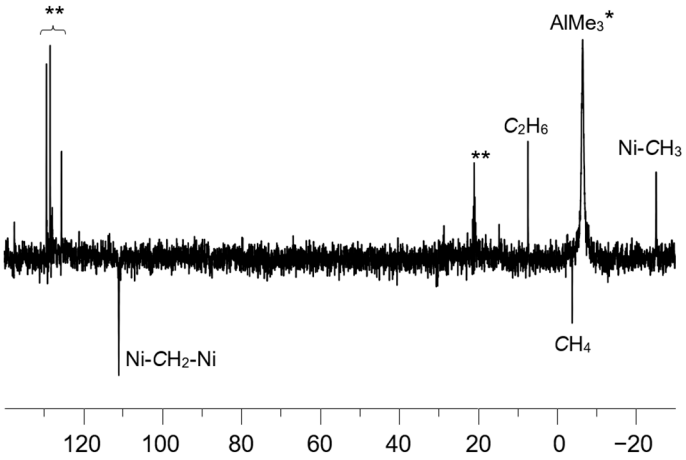

Figure 5. dept135 ^{13}C NMR spectrum (toluene-d_8, [Al]/[Ni] = 10/1, C_{Ni} = 5 mM, 0 °C) of the sample **1**/$AlMe_3$*. $AlMe_3$* is a trimethylaluminum enriched by ^{13}C isotope (ca. 54 at.%). Doubled asterisks mark solvent (toluene-d_8) resonances.

Each of the remaining two resonances at δ 5.44 (br. d, $^2J_{HH}$ = 3.5 Hz, 1H) and δ 3.72 (br. d, $^2J_{HH}$ = 3.5 Hz, 1H) has an integral intensity corresponding to one hydrogen atom (Figure 4a). The ^1H-^1H COSY NMR spectrum of **2** displays a couple of cross-peaks (Figure S1 in SM), corresponding to spin-spin coupling between these protons.

Using ^{13}C-enriched trimethylaluminum instead of $Al(^{12}CH_3)_3$ leads to the appearance of two additional doublets at δ 5.44 and δ 3.72 in ^1H NMR due to one-bond ^{13}C-^1H spin-spin coupling $^1J_{CH}$ = 132.6 Hz and $^1J_{CH}$ = 142.8 Hz, respectively (Figure 4a,b). Note that broadened doublets δ 5.44 ($^1J_{HH}$ = 3.5 Hz) and δ 3.72 ($^1J_{HH}$ = 3.5 Hz) are also observed due to the presence of $Al(^{12}CH_3)_3$ in partially labeled sample.

The resonance of the CH_2-group with an integral intensity equal to those of Ni-CH_3 was detected in the $^{13}C\{^1H\}$ dept135 NMR spectrum of the sample **1**/$AlMe_3$* at δ 111.1 (Figure 5). The cross peaks in 2D ^1H,^{13}C NMR clearly indicated the correlation of ^{13}C resonance at δ 111.1 and two ^1H resonances at δ 5.44 and δ 3.72, respectively (Figure S2 in SM).

Only the initial α-diimine ligand containing no ^{13}C-lables was recovered after **1**/$AlMe_3$* sample hydrolysis with H_2O, followed by extraction with Et_2O, and drying. Therefore, the resonances at δ 5.44 and δ 3.72 in the ^1H NMR spectrum and at δ 111.1 in the ^{13}C NMR one undoubtedly belong to the CH_2-group bound to the Ni center (or centers) rather than to the α-diimine ligand. The $^2J_{HH}$ coupling constant of 3.5 Hz is lower than expected for heminal protons at sp^3 hybrid carbon atoms, but reasonably higher than those for heminal protons at sp^2 carbon atoms [65].

Further, the ^{13}C NMR chemical shift of the CH_2 group (δ 111.1) is not characteristic of nickel(II)-bonded sp^3-carbons of Ni-CH_2-R moiety (such carbons display ^{13}C NMR resonances typically in the range of 10 . . . 20 ppm; see ref. [38,59]). Unfortunately, ^{13}C NMR data on the species containing Ni=CH_2 moieties are lacking, which complicates speculating on the characteristic values of ^{13}C chemical shifts of the sp^2 carbons directly bonded to the Ni center. However, a number of nickel(II) complexes of chelating *N*-heterocyclic carbenes are well-known (see Refs. [66,67], and references therein). For these compounds, ^{13}C NMR chemical shifts of the sp^2 carbons directly bonded to the Ni center fall within the range from 180 . . . 200 ppm. Therefore, the value of δ 111.1 might be tentatively attributed to the carbon of Ni-CH_2 moiety with the hybridization intermediate between sp^3 and sp^2.

It is reasonable to conclude that **2** is a dinuclear Ni(II)-Ni(II) complex rather than mononuclear one. Indeed, in the case of mononuclear Ni(II) species, six-coordinated Ni(II) center supported by two bidentate α-diimine ligands, one methyl, and one CH_2-group does not have square-planar geometry and thus would not display the ^1H NMR spectrum characteristic of diamagnetic species. We assume that complex **2** may be represented as alternative resonance structures differing in the mode of Br ligation (outer-sphere or

inner-sphere, Figure 6). To discriminate between these alternatives, quantum-chemical calculations have been performed (see below).

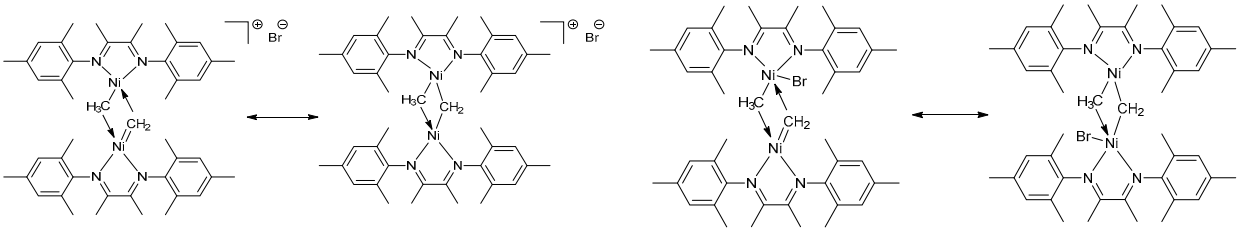

Figure 6. Proposed resonance structures for **2**.

2.3. DFT Calculations

To discriminate between the two possible structures of **2** (Figure 6), we have calculated the geometries and free energies of the bridged homodinuclear complex at the UB3LYP-D3/def2-TZVPP level of theory, which was previously shown to satisfactorily predict the gaps between different spin states of first-row transition metal complexes [68–70]. Crucially, starting from the draft structure [L(Me)Ni^{II}(μ-CH_2)Ni^{II}(Br)L], optimization led to the doubly bridged ion pairs of the type [LNi^{II}(μ-Me)(μ-CH_2)Ni^{II}L]$^+Br^-$, thus favoring the assignment of **2** to the ion-pair structure (Figure 6). Singlet (S = 0) appeared to be 11.8 kcal/mol lower in energy than its triplet (S = 1) counterpart (for the energies, molecular models and Cartesian coordinates see SM), which is consistent with the diamagnetic nature of species **2** as evident from NMR data.

2.4. Temperature Behavior of the Ortho-Methyl and Meta-H Resonances

The molecule of **2** is not symmetric, so magnetic non-equivalence of the ligand protons is expected. Hindered rotation of the mesityl moieties around the C-N bound leads to a number of resonances of non-equivalent *o*-methyl and *m*-H resonances in the ^{1}H NMR at low temperatures (namely at −20 and 0 °C; Figures 2c and 3a). Sample heating partially unfreezes rotation around the N-C bond, leading to slow or moderate exchange at 25 °C; it causes dramatic broadening of the resonances mentioned above. At T = 40 °C, the *m*-H resonances collapse, giving rise to a narrow singlet indicative of fast exchange. Further temperature increase leads to decomposition of **2**, which prevents detection of narrow resonances of the *o*-Me groups.

2.5. The Role of 2 in Catalytic Process

It is interesting to establish the role of **2** in ethylene polymerization. The real catalytic experiments in autoclave usually require using high excess of co-catalyst (Al/Ni = 500 or more), which in additions acts as a scavenger. As an example, the results of the ethylene polymerization over **1**/$AlMe_3$ (Al/Ni = 500) catalyst system are summarized in Table 1 [51].

Table 1. Data of the ethylene polymerization over 1/$AlMe_3$ catalyst system [a].

System	[Al]/[Ni]	Activity, kg (PE)·mol_{Ni}^{-1}·h^{-1}	M_w, g/mol	M_n, g/mol	M_w/M_n	Branches/1000 C
1/$AlMe_3$	500	27,000	78,000	39,000	2.0	36 ± 2

[a] Polymerization conditions: toluene (100 mL); time 60 min; T = 50 °C; P(C_2H_4) = 5 bar; 2.0 μmol of pre-catalyst **1**.

Unfortunately, under these conditions the Ni(II) species are not stable, undergoing rapid reduction into the corresponding Ni(I) counterparts (neutral heterobinuclear complexes of [LNi^I(μ-Me)$_2$$AlMe_2$], [51]) predominating in the resulting reaction solution. That is why we have performed the following NMR-tube catalytic experiment instead. First, species **2** was generated in the **1**/$AlMe_3$ sample (toluene-d_8, [Al]/[Ni] = 10/1, C_{Ni} = 5 mM).

Then, ethylene was bubbled through the sample during 1 min at 0 °C, and NMR and EPR spectra were recorded right after. This was repeated five times.

According to the ^{1}H NMR and EPR data, after each bubbling ethylene was completely polymerized, the concentration of **2** decreased, and EPR-resonances of Ni(I) species grew up (Figures S3 and S4 in SM). After the 3rd cycle, NMR resonances of **2** disappeared completely, but the sample kept its ethylene polymerization activity. This is not surprising, given the reported ability of monovalent nickel species ([LNi^{I}(μ-Me)$_2$AlMe$_2$]) to give rise to polymerization-active species in the presence of excess of ethylene [51].

Altogether, **2** can be assigned to a resting state of the true catalytically active species, yet currently, it is not clear whether **2** converts into the active species directly or through monomeric nickel(I) species of the type [LNi^{I}(μ-Me)$_2$AlMe$_2$]. Possible transformations of the nickel species in the catalyst system **1**/AlMe$_3$ are presented in Scheme 1.

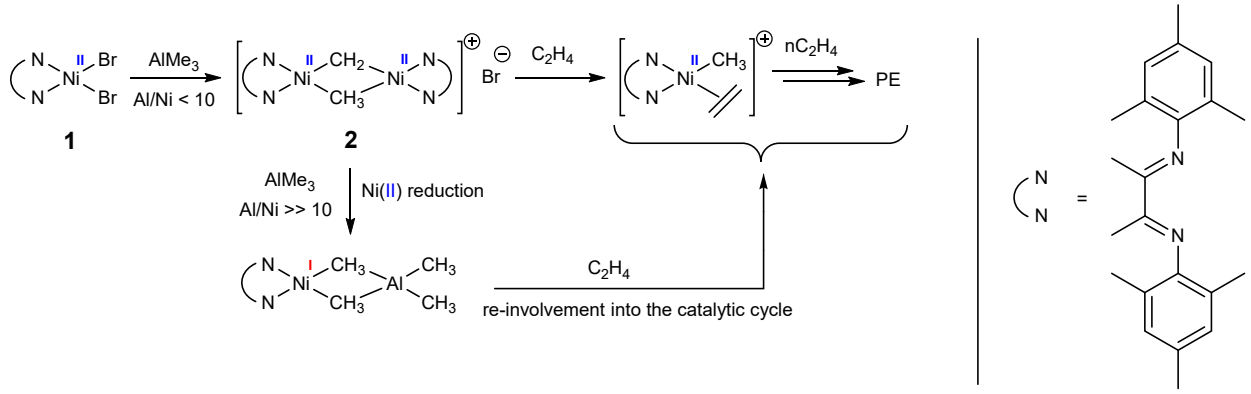

Scheme 1. Possible transformations of the nickel species in the catalyst system **1**/AlMe$_3$.

3. Materials and Methods

3.1. General Procedures

Toluene-d$_8$ and 1.2-difluorobenzene (Aldrich, St. Louis, MO, USA) were dried over molecular sieves (4 Å), degassed in a vacuum, and stored under dry argon. Methylene chloride, CDCl$_3$, and CD$_2$Cl$_2$ (Aldrich) were dried over P$_2$O$_5$, distilled, and stored under dry argon. Hexane was stored over molecular sieves (4 Å), purified by refluxing over sodium-benzophenone and distilled in dry argon. AlMe$_3$ (neat), 1,2-butanedione, 2,4,6-trimethylaniline, 2,6-dimethylaniline, NiBr$_2$(DME), D$_2$O (99 at.% of D), and CH$_3$OD (99 at.% of D) were purchased from Aldrich and used without preliminary purification. Al(^{13}CH$_3$)$_3$ was prepared from ^{13}C-labelled CH$_3$I (Aldrich) by sequential treatments with Al metal at 80 °C and Na metal in C$_{12}$H$_{26}$ at 100 °C and isolated by vacuum distillation [71]. All operations with oxygen-sensitive and moisture-sensitive compounds were carried out under dry argon atmosphere by using standard Schlenk techniques (synthesis of nickel complexes) or glovebox (preparing the samples for NMR and EPR experiments).

3.2. NMR and EPR Spectra Registration

^{1}H, ^{2}H and ^{13}C NMR spectra were recorded on a Bruker Avance 400 MHz NMR spectrometer (Rheinstetten, Germany) in 5 mm (o.d.) NMR tubes at 400.130, 61.422, and 100.613 MHz, respectively. Typical operating conditions for ^{1}H NMR measurements were as follows: spectral width 4–5 kHz for diamagnetic and 40 kHz for paramagnetic compounds; spectrum accumulation frequency 0.25–0.4 Hz; 32–64 transients, 90° pulse at 12.0 μs. Operating conditions for ^{2}H NMR experiment: spectral width 1 kHz; spectrum accumulation frequency 0.5 Hz; 8000 transients, 90° pulse at 6.6 μs. Operating conditions for ^{13}C NMR experiments: spectral width 20 kHz; spectrum accumulation frequency 0.2–0.01 Hz; 32–2000 transients, 45° pulse at 3.8 μs. Multiplicities and J_{CH} coupling constants were determined from gated decoupled spectra. ^{1}H-^{1}H and ^{13}C-^{1}H correlations were established by using standard Bruker cosydfqf and hxdeptbiqf pulse programs, respectively. For calculations of ^{1}H chemical shifts (ppm), the resonances of the residual solvent protons (δ

2.09 for C*H*$D_2C_6D_5$, δ 7.26 for C*H*Cl_3, and δ 5.27 for C*H*DCl_2) were used. ^{2}H chemical shifts were referred to the signal of C*D*$H_2C_6H_5$ in toluene (δ 2.10) whereas ^{13}C ones were referred to the solvent resonances (δ 77.16 for *C*DCl_3 and δ 20.4 for *C*D_3-group of toluene-d_8). The sample temperature measurement uncertainty and temperature reproducibility were less than ±1 °C.

EPR spectra were recorded on a CMS 8400 EPR spectrometer (Adani, Minsk, Belarus) at 9.44 GHz, modulation frequency 100 kHz, modulation amplitude 0.5 mT. Frozen solution EPR measurements were conducted in a quartz finger Dewar filled with liquid nitrogen (−196 °C). Toluene solution of TEMPO (2 mM) was used as an external standard for *g*-values calculations.

Samples **1**/$AlMe_3$ (**1′**/$AlMe_3$, or $\mathbf{1^D}$/$AlMe_3$) were prepared in the argon-filled glovebox by simple reagents mixing at ambient temperatures. Septum stoppers and Parafilm "M" were used to avoid oxygen/moisture transfer into the NMR tube.

3.3. Synthesis of the Complexes **1**, **1′**, *and* $\mathbf{1^D}$

In general, complexes **1**, **1′**, and $\mathbf{1^D}$ were synthesized according to published procedures (see, for example, ref. [72]) with small deviations.

3.3.1. Synthesis of *1,4-Bis-2,4,6-trimethylphenyl-2,3-dimethyl-1,4-diazabuta-1,3-diene* (**L1**)

To a stirred solution of 2,3-butanedione (100 mg, 1.16 mmol) in methanol (2 mL), a solution of 2,4,6-trimethylaniline (170 mg, 1.26 mmol) in methanol (3 mL) was added. After the addition of a droplet of glacial acetic acid, reaction mixture was refluxed overnight. After reaction mixture cooling to room temperature the solvent was removed in a vacuum to give a yellow powder of crude ligand **L1**. Further recrystallization from ethanol afforded bright yellow crystals of pure **L1** (242 mg, 65% yield).

^{1}H NMR (24 °C, $CDCl_3$): δ 6.91 (s, 4H, Ar-*H*$_m$), 2.31 (s, 6H, Ar-C*H*$_{3\,p}$), 2.06 (s, 6H, N=C-C*H*$_3$), 2.02 (s, 12H, Ar-C*H*$_{3\,o}$). ^{13}C NMR (24 °C, $CDCl_3$): δ 168.50 (2C, N=C-CH_3), 145.99 (2C, Ar-C_{ip}), 132.55 (2C, Ar-C_p), 128.71 (4C, Ar-C_m, $^1J_{CH}$ = 154.6 Hz), 124.68 (4C, Ar-C_o), 20.86 (2C, Ar-C*H*$_{3\,p}$, $^1J_{CH}$ = 126.3 Hz), 17.86 (4C, Ar-C*H*$_{3\,o}$, $^1J_{CH}$ = 126.7 Hz), 15.93 (2C, N=C-C*H*$_3$, $^1J_{CH}$ = 128.6 Hz). Anal. Calcd. for $C_{22}H_{28}N_2$: C, 82.45; H, 8.81; N, 8.74. Found: C, 82.54; H, 8.96; N, 8.75.

3.3.2. Synthesis of *1,4-Bis-2,6-dimethylphenyl-2,3-dimethyl-1,4-diazabuta-1,3-diene* (**L1′**)

L1′ was obtained according to the procedure described above (2,6-dimethylaniline was used instead of mesitylamine) as bright yellow crystals in 61% yield.

^{1}H NMR (24 °C, $CDCl_3$): δ 7.08 (d, 4H, Ar-*H*$_m$, $^3J_{HH}$ = 7.7 Hz), 6.95 (t, 2H, Ar-*H*$_p$, $^3J_{HH}$ = 7.7 Hz), 2.06 (s, 6H, N=C-C*H*$_3$), 2.05 (s, 12H, Ar-C*H*$_{3\,o}$). ^{13}C NMR (24 °C, $CDCl_3$): δ 168.25 (2C, N=*C*-CH_3), 148.43 (2C, Ar-C_{ip}), 128.08 (4C, Ar-C_m, $^1J_{CH}$ = 158.7 Hz), 124.83 (4C, Ar-C_o,), 123.42 (2C, Ar-C_p, $^1J_{CH}$ = 160.3 Hz), 17.93 (4C, Ar-C*H*$_{3\,o}$, $^1J_{CH}$ = 126.8 Hz), 15.99 (2C, N=C-*C*H$_3$, $^1J_{CH}$ = 128.9 Hz). Anal. Calcd. for $C_{20}H_{24}N_2$: C, 82.15; H, 8.27; N, 9.58. Found: C, 82.21; H, 8.54; N, 9.60.

3.3.3. Synthesis of ^{2}*H-Enriched 2,3-butanedione*

^{2}H-enriched 2,3-butanedione was prepared by H/D exchange between 2,3-butanedione and D_2O according to a published procedure [73]. To a stirred solution of 2,3-butanedione (2.00 g, 23.5 mmol) in D_2O (99% of D, 10 mL, 495 mmol), concentrated hydrochloric acid (0.8 mL, 10 mmol) was added dropwise. The reaction mixture was allowed to stir for 10 days at ambient temperature. After that, acid was neutralized by addition of $CaCO_3$ powder (2 g, 20 mmol), and the product was extracted by CH_2Cl_2 (3 × 15 mL). Combined organic phase was dried over Na_2SO_4 and filtered. Pure ^{2}H-enriched 2,3-butanedione (84 at. % of ^{2}H) was isolated by distillation (1.45 g, 19.3 mmol, 82% yield). Deuterium abundance in the product was determined by ^{1}H NMR. ^{1}H NMR (25 °C, $CDCl_3$): δ 2.33 (s, C*H*$_3$), 2.31 (t, C*H*$_2$D, $^2J_{HD}$ = 2.2 Hz), 2.29 (quint, C*H*D_2, $^2J_{HD}$ = 2.2 Hz).

3.3.4. Synthesis of ^{2}*H-Enriched 1,4-bis-2,4,6-trimethylphenyl-2,3-dimethyl-1,4-diazabuta-1,3-diene* (**L1^{D}**)

According to the procedure described for **L1**, the desired ligand **L1^{D}** was obtained as bright yellow crystals in 65% yield. To avoid isotopic exchange between ^{2}H-enriched 2,3-butanedione and OH-groups of methanol during synthesis, CH_3OD was used as solvent instead. Deuterium abundance in the N=C-Me moiety of the resulting ligand was 84 at. %.

^{1}H NMR (25 °C, $CDCl_3$): δ 6.91 (s, 4H, Ar-H_m), 2.31 (s, 6H, Ar-C$H_{3\,p}$), 2.06–2.03 (m, 0.9H, N=C-CH_3 + N=C-CH_2D + N=C-CHD$_2$), 2.02 (s, 12H, Ar-C$H_{3\,o}$).

3.3.5. Synthesis of *1,4-Bis-2,4,6-trimethylphenyl-2,3-dimethyl-1,4-diazabuta-1,3-diene nickel(II) dibromide* (complex **1**)

All manipulations were performed under dry argon atmosphere using the standard Schlenk technique. Only solvents containing no water and oxygen traces were used.

A Schlenk flack was charged by a freshly prepared solution of **L1** (100 mg, 0.31 mmol) in CH_2Cl_2 (10 mL). A preliminary weighted (in glovebox) amount of $NiBr_2$(DME) (100 mg, 0.32 mmol) was added rapidly and reaction mixture was allowed to stir overnight at ambient temperature. After that insoluble compounds were filtered off and filtrate was dried in vacuum. The resulting dark-red powder was recrystallized from CH_2Cl_2/hexane to give red crystals of pure **1** (119 mg, 0.22 mmol, 70% yield).

^{1}H NMR (25 °C, CD_2Cl_2): δ 34.8 (br, 6H, Ar-C$H_{3\,p}$, $\Delta\nu_{1/2}$ = 33 Hz), 27.9 (br, 12H, Ar-C$H_{3\,o}$, $\Delta\nu_{1/2}$ = 100 Hz), 24.1 (br, 4H, Ar-H_m, $\Delta\nu_{1/2}$ = 25 Hz), −21.2 (br, 6H, N=C-CH_3, $\Delta\nu_{1/2}$ = 48 Hz). Anal. Calcd. for $C_{22}H_{28}N_2Br_2Ni$: C, 49.03; H, 5.24; N, 5.20; Br, 29.65; Ni, 10.89. Found: C, 50.35; H, 6.15; N, 5.26.

3.3.6. Synthesis of *1,4-Bis-2,6-dimethylphenyl-2,3-dimethyl-1,4-diazabuta-1,3-diene nickel(II) dibromide* (complex **1′**)

Complex **1′** (dark red crystals) was prepared in a similar manner by using the corresponding α-diimine ligand **L1′** in 78% yield.

^{1}H NMR (24 °C, $CDCl_3$): δ 28.2 (br, 12H, Ar-C$H_{3\,o}$, $\Delta\nu_{1/2}$ = 134 Hz), 24.1 (br, 4H, Ar-H_m, $\Delta\nu_{1/2}$ = 61 Hz), −17.6 (br, 2H, Ar-H_p, $\Delta\nu_{1/2}$ = 74 Hz), −22.7 (br, 6H, N=C-CH_3, $\Delta\nu_{1/2}$ = 66 Hz). Anal. Calcd. for $C_{20}H_{24}N_2Br_2Ni$: C, 47.02; H, 4.73; N, 5.48; Br, 31.28; Ni, 11.49. Found: C, 47.48; H, 5.18; N, 5.46.

3.3.7. Synthesis of ^{2}*H-Enriched 1,4-bis-2,6-dimethylphenyl-2,3-dimethyl-1,4-diazabuta-1,3-diene nickel(II) dibromide* (complex **1^{D}**)

Dark red crystals of **1^{D}** were obtained in a similar manner by using the corresponding ^{2}H-enriched α-diimine ligand **L1^{D}** in 72% yield.

^{1}H NMR (25 °C, CD_2Cl_2): δ 34.9 (br, 6H, Ar-C$H_{3\,p}$, $\Delta\nu_{1/2}$ = 35 Hz), 27.9 (br, 12H, Ar-C$H_{3\,o}$, $\Delta\nu_{1/2}$ = 105 Hz), 24.1 (br, 4H, Ar-H$_m$, $\Delta\nu_{1/2}$ = 30 Hz), −21.4 (br, N=C-CH_3, $\Delta\nu_{1/2}$ = 50 Hz), −22.2 (br, N=C-CH_2D, $\Delta\nu_{1/2}$ = 55 Hz), −22.0 (br, N=C-CHD$_2$, $\Delta\nu_{1/2}$ = 50 Hz). Overall integral intensity of N=C-*Me* moiety corresponds to 0.9 H.

3.4. DFT Calculations: Computational Details

Geometry optimization and frequency analysis of **2** with different multiplicities (S = 0, S = 1; for the (S = 2) spin isomer, the calculation did not converge) were carried with the UB3PLYP density functional theory scheme (DFT) with D3 corrections [74] using GAUSSIAN 16 program suite [75], with the def2-TZVPP [76] basis set for the Ni and Br atom and 6-311G(d) [77] basis set for other atoms. Solvation effects (with toluene) were incorporated using polarized continuum model (PCM) method [78,79] as implemented in GAUSSIAN 16. The stationary points were ascertained by vibrational frequency analysis with no imaginary frequencies. The Gibbs energies reported in this paper were sum of electronic and thermal free energies. DFT optimized Cartesian coordinates and potential energies (Ha) for the calculated structures are presented in the SM.

4. Conclusions

A novel diamagnetic species **2** was detected upon activation of Brookhart-type Ni(II) α-diimine ethylene polymerization pre-catalyst **1** ($LNiBr_2$, L = 1,4-bis-2,4,6-trimethylphenyl-2,3-dimethyl-1,4-diazabuta-1,3-diene) with $AlMe_3$ co-catalyst. At [Al]:[Ni] ratio of 10:1, species **2** is room-temperature stable and accounts for the major part of nickel. ^1H, ^2H, and ^{13}C NMR spectroscopic characterization of **2** has witnessed its dinuclear nature, incorporating two antiferromagnetically coupled Ni(II) centers, to give an overall $S = 0$ spin state. DFT calculations allow to reasonably discriminate between the two possible structures, $[L(Me)Ni^{II}(\mu\text{-}CH_2)Ni^{II}(Br)L]$ and $[LNi^{II}(\mu\text{-}Me)(\mu\text{-}CH_2)Ni^{II}L]^+Br^-$, favoring the latter, doubly bridged outer-sphere ion pair structure. Complex **2** is sufficiently stable in the reaction solution only at low Al/Ni molar ratios, while in conditions approaching those of practical polymerization ([Al]:[Ni] = 500), quantitative reduction of Ni(II) to the monovalent state takes place. Most plausibly, **2** can be assigned to a resting state of the true Ni(II) active sites of ethylene polymerization.

Supplementary Materials: The following supporting information can be downloaded at: https://www.mdpi.com/article/10.3390/catal13020333/s1, Figure S1: ^1H-^1H cosydfph NMR spectrum of the sample **1**/$AlMe_3$; Figure S2: ^1H-^{13}C hxdeptbiqf NMR spectrum of the sample **1**/$AlMe_3$; Figure S3: ^1H NMR spectra of the catalyst system **1**/$AlMe_3$/C_2H_4; Figure S4: EPR spectra of the catalyst system **1**/$AlMe_3$/C_2H_4; Table S1: The integral intensities of ^1H NMR resonances of **2**; Cartesian coordinates and calculated energies.

Author Contributions: Conceptualization, I.E.S., K.P.B. and E.P.T.; Synthesis of Ni(II) complexes and samples preparing, A.A.A. and N.V.S.; NMR spectroscopic studies, I.E.S.; DFT calculations, A.A.B.; writing—original draft preparation, I.E.S.; writing—review and editing, I.E.S., K.P.B. and E.P.T.; project administration, K.P.B. and E.P.T.; funding acquisition, I.E.S. All authors have read and agreed to the published version of the manuscript.

Funding: This work was supported by the Russian Science Foundation, grant number # 22-23-00048.

Data Availability Statement: Not applicable.

Acknowledgments: The authors thank D.E. Babushkin for the synthesis of $Al(^{13}CH_3)_3$. NMR experiments were conducted using the equipment of the Department of Mechanisms of Catalytic Reactions, Boreskov Institute of Catalysis. AAB acknowledges the access to the supercomputer facilities of the Computing Centre of Novosibirsk State University.

Conflicts of Interest: The authors declare no conflict of interest.

References

1. Tan, C.; Zou, C.; Chen, C. An Ionic Cluster Strategy for Performance Improvements and Product Morphology Control in Metal-Catalyzed Olefin-Polar Monomer Copolymerization. *J. Am. Chem. Soc.* **2022**, *144*, 2245–2254. [CrossRef]
2. Zhang, Y.; Kang, X.; Jian, Z. Selective branch formation in ethylene polymerization to access precise ethylene-propylene copolymers. *Nat. Commun.* **2022**, *13*, 725. [CrossRef] [PubMed]
3. Zhu, N.; Asadullah Khan, M.; Pang, W.; Behzadi, S.; Qasim, M. Synthesis of Ultra-High molecular weight polyethylene elastomers by para-tert-Butyl dibenzhydryl functionalized α-Diimine nickel catalysts at elevated temperature. *Eur. Pol. J.* **2022**, *178*, 111497. [CrossRef]
4. Wang, Q.; Zhang, Z.; Zou, C.; Chen, C. A general cocatalyst strategy for performance enhancement in nickel catalyzed ethylene (co)polymerization. *Chin. Chem. Lett.* **2022**, *33*, 4363–4366. [CrossRef]
5. Hu, X.; Kang, X.; Jian, Z. Suppression of Chain Transfer at High Temperature in Catalytic Olefin Polymerization. *Angew. Chem. Int. Ed.* **2022**, *61*, e202207363. [CrossRef] [PubMed]
6. Lu, W.; Liao, Y.; Dai, S. Facile access to ultra-highly branched polyethylenes using hybrid "sandwich" Ni(II) and Pd(II) catalysts. *J. Catal.* **2022**, *411*, 54–61. [CrossRef]
7. Lu, Z.; Liao, Y.; Fan, W.; Dai, S. Efficient suppression of the chain transfer reaction in ethylene coordination polymerization with dibenzosuberyl substituents. *Polym. Chem.* **2022**, *13*, 4090–4099. [CrossRef]
8. Zhang, Q.; Liu, M.; Ma, Y.; Ye, Z.; Liang, T.; Sun, W.H. Highly active and thermostable camphyl α-diimine–nickel(II) catalysts for ethylene polymerization: Effects of N-aryl substituting groups on catalytic properties and branching structures of polyethylene. *Appl. Organomet. Chem.* **2022**, *36*, e6606. [CrossRef]

9. Lei, T.; Ma, Z.; Liu, H.; Wang, X.; Li, P.; Wang, F.; Wu, W.; Zhang, S.; Xu, G.; Wang, F. Preparation of highly branched polyolefins by controlled chain-walking olefin polymerization. *Appl. Organomet. Chem.* **2022**, *36*, e6788. [CrossRef]
10. Lu, Z.; Chang, G.; Wang, H.; Jing, K.; Dai, S. A Dual Steric Enhancement Strategy in α-Diimine Nickel and Palladium Catalysts for Ethylene Polymerization and Copolymerization. *Organometallics* **2022**, *41*, 124–132. [CrossRef]
11. Doerr, A.M.; Curry, M.R.; Chapleski, R.C.; Burroughs, J.M.; Lander, E.K.; Roy, S.; Long, B.K. Redox Potential as a Predictor of Polyethylene Branching Using Nickel α-Diimine Catalysts. *ACS Catal.* **2022**, *12*, 73–81. [CrossRef]
12. Chen, M.; Chen, C. Nickel catalysts for the preparation of functionalized polyolefin materials. *Chin. Sci. Bull.* **2022**, *67*, 1881–1894. [CrossRef]
13. Zheng, H.; Li, Y.; Du, W.; Cheung, C.S.; Li, D.; Gao, H.; Deng, H.; Gao, H. Unprecedented Square-Planar α-Diimine Dibromonickel Complexes and Their Ethylene Polymerizations Modulated by Ni–Phenyl Interactions. *Macromolecules* **2022**, *55*, 3533–3540. [CrossRef]
14. Yan, M.; Kang, X.; Li, S.; Xu, X.; Luo, Y.; He, S.; Chen, C. Mechanistic Studies on Nickel-Catalyzed Ethylene Polymerization: Ligand Effects and Quantitative Structure–Activity Relationship Model. *Organometallics* **2022**, *41*, 3212–3218. [CrossRef]
15. Antonov, A.A.; Bryliakov, K.P. Post-metallocene catalysts for the synthesis of ultrahigh molecular weight polyethylene: Recent advances. *Eur. Polymer J.* **2021**, *142*, 110162. [CrossRef]
16. Liang, T.; Goundari, S.B.; Chen, C. A simple and versatile nickel platform for the generation of branched high molecular weight polyolefins. *Nat. Commun.* **2020**, *11*, 372. [CrossRef] [PubMed]
17. Xia, J.; Zhang, Y.X.; Kou, S.Q.; Jian, Z.B. A concerted double-layer steric strategy enables an ultra-highly active nickel catalysts to access ultrahigh molecular weight polyethylenes. *J. Catal.* **2020**, *90*, 30–36. [CrossRef]
18. Tran, Q.H.; Brookhart, M.; Daugulis, O. New neutral nickel and palladium sandwich catalysts: Synthesis of ultrahigh molecular weight polyethylene (UHMWPE) via highly controlled polymerization and mechanistic studies of chain propagation. *J. Am. Chem. Soc.* **2020**, *142*, 7198–7206. [CrossRef]
19. Li, S.K.; Xu, S.Y.; Dai, S.Y. A remote nonconjugated electron effect in insertion polymerization with α-diimine nickel and palladium species. *Polym. Chem.* **2020**, *11*, 2692–2699. [CrossRef]
20. Muhammad, Q.; Tan, C.; Chen, C.L. Concerted steric and electronic effects on α-diimine nickel- and palladium-catalyzed ethylene polymerization and copolymerization. *Sci. Bull.* **2020**, *65*, 300–307. [CrossRef] [PubMed]
21. Hu, X.Q.; Zhang, Y.X.; Jian, Z.B. Unsymmetrical strategy makes significant differences in α-diimine nickel and palladium catalyzed ethylene copolymerizations. *ChemCatChem* **2020**, *12*, 2497–2505. [CrossRef]
22. Tan, C.; Chen, C.L. Emerging palladium and nickel catalysts for copolymerization of olefins with polar monomers. *Angew. Chem. Int. Ed.* **2019**, *58*, 7192–7200. [CrossRef]
23. Gong, Y.F.; Li, S.K.; Gong, Q.; Zhang, S.J.; Liu, B.Y.; Dai, S.Y. Systematic investigations of ligand steric effects on α-diimine nickel catalyzed olefin polymerization and copolymerization. *Organometallics* **2019**, *38*, 2919–2926. [CrossRef]
24. Soshnikov, I.E.; Bryliakov, K.P.; Antonov, A.A.; Talsi, E.P. Ethylene polymerization of nickel catalysts with α-diimine ligands: Factors controlling the structure of active species and polymer properties. *Dalton Trans.* **2019**, *48*, 7974–7984. [CrossRef] [PubMed]
25. Chen, Z.; Brookhart, M. Exploring ethylene/polar vinyl monomer copolymerizations using Ni and Pd α-diimine catalysts. *Acc. Chem. Res.* **2018**, *51*, 1831–1839. [CrossRef]
26. Fang, J.; Sui, X.L.; Li, Y.G.; Chen, C.L. Synthesis of polyolefin elastomers from unsymmetrical α-diimine nickel catalyzed olefin polymerization. *Polym. Chem.* **2018**, *30*, 4143–4149. [CrossRef]
27. Zhong, L.; Li, G.L.; Liang, G.D.; Gao, H.Y.; Wu, Q. Enhancing thermal stability and living fashion in α-diimine-nickel catalyzed (co)polymerization of ethylene and polar monomers by increasing the steric bulk of ligand backbone. *Macromolecules* **2017**, *50*, 2675–2682. [CrossRef]
28. Wang, Z.; Liu, Q.B.; Solan, G.A.; Sun, W.-H. Recent advances in Ni_{imine}-donor ligand effects on catalytic activity, thermal stability and oligo-/polymer structure. *Coord. Chem. Rev.* **2017**, *350*, 68–83. [CrossRef]
29. Svejda, S.A.; Johnson, L.K.; Brookhart, M. Low-Temperature Spectroscopic Observation of Chain Growth and Migratory Insertion Barriers in (α-Diimine)Ni(II) Olefin Polymerization Catalysts. *J. Am. Chem. Soc.* **1999**, *121*, 10634–10635. [CrossRef]
30. Leatherman, M.D.; Svejda, S.A.; Johnson, L.K.; Brookhart, M. Mechanistic Studies of Nickel(II) Alkyl Agostic Cations and Alkyl Ethylene Complexes: Investigations of Chain Propagation and Isomerization in (α-diimine)Ni(II)-Catalyzed Ethylene Polymerization. *J. Am. Chem. Soc.* **2003**, *125*, 3068–3081. [CrossRef]
31. Meinhard, D.; Reuter, P.; Rieger, B. Activation of Polymerization Catalysts: Synthesis and Characterization of Novel Dinuclear Nickel(I) Diimine Complexes. *Organometallics* **2007**, *26*, 751–754. [CrossRef]
32. Kraikivskii, P.B.; Saraev, V.V.; Bocharova, V.V.; Romanenko, G.V.; Matveev, D.A.; Petrovskii, S.K.; Kuzakov, A.S. Nickel(I) Complex as the Final Product of the Sequence of Spontaneous Transformations in the System $Ni(Allyl)_2$–(2,6-Diisopropylphenyl)diazabutadiene. *Rus. J. Coord. Chem.* **2012**, *38*, 416–425. [CrossRef]
33. Petrovskii, S.K.; Saraev, V.V.; Kraikivskii, P.B.; Gurinovich, N.S.; Matveev, D.A.; Bocharova, V.V. Formation of paramagnetic intermediates under the conditions of Brookhart-type catalyst activation and operation. *Rus. Chem. Bull. Int. Ed.* **2013**, *62*, 1323–1326. [CrossRef]
34. Gao, W.; Xin, L.; Hao, Z.; Li, G.; Su, J.H.; Zhou, L.; Mu, Y. The ligand redox behavior and role in 1,2-bis[(2,6-diisopropylphenyl)imino]-acenaphthene nickel-TMA(MAO) systems for ethylene polymerization. *Chem. Commun.* **2015**, *51*, 7004–7007. [CrossRef]

35. Zhao, Y.; Wang, Z.; Jing, X.; Dong, Q.; Gong, S.; Li, Q.S.; Zhang, J.; Wua, B.; Yang, X.J. α-Diimine nickel complexes of ethylene and related alkenes. *Dalton Trans.* **2015**, *44*, 16228–16232. [CrossRef]
36. Anderson, W.C., Jr.; Rhinehart, J.L.; Tennyson, A.G.; Long, B.K. Redox-Active Ligands: An Advanced Tool To Modulate Polyethylene Microstructure. *J. Am. Chem. Soc.* **2016**, *138*, 774–777. [CrossRef]
37. Gurinovich, N.S.; Petrovskii, S.K.; Saraev, V.V.; Salii, I.V. Study of the Nature and Mechanism of the Formation of Paramagnetic Species in Nickel-Based Brookhart-Type Catalytic Systems. *Kin. Catal.* **2016**, *57*, 523–527. [CrossRef]
38. Xu, H.; White, P.B.; Hu, C.; Diao, T. Structure and Isotope Effects of the β-H Agostic (α-diimine)Nickel Cation as a Polymerization Intermediate. *Angew. Chem. Int. Ed.* **2017**, *56*, 1535–1538. [CrossRef] [PubMed]
39. Gomes, C.S.B.; Ribeiro, A.F.G.; Fernandes, A.C.; Bento, A.; Ribeiro, M.R.; Kociok-Köhn, G.; Pascu, S.I.; Duarte, M.T.; Gomes, P.T. Reactivity of cationic α-diimine cyclopentadienyl nickel complexes towards $AlEt_2Cl$: Synthesis, characterization and ethylene polymerization. *Catal. Sci. Technol.* **2017**, *7*, 3128–3142. [CrossRef]
40. Anderson, W.C., Jr.; Park, S.H.; Brown, L.A.; Kaiser, J.M.; Long, B.K. Accessing Multiple Polyethylene Grades Via a Single Redox-Active Olefin Polymerization Catalyst. *Inorg. Chem. Front.* **2017**, *4*, 1108–1112. [CrossRef]
41. Ahmadjo, S.; Damavandi, S.; Zohuri, G.H.; Farhadipour, A.; Samadieh, N.; Etemadinia, Z. Synthesis and application of fluorinated a-diimine nickel catalyst for ethylene polymerization: Deactivation mechanism. *Polym. Bull.* **2017**, *74*, 3819–3832. [CrossRef]
42. Chen, Z.; Leatherman, M.D.; Daugulis, O.; Brookhart, M. Nickel-Catalyzed Copolymerization of Ethylene and Vinyltrialkoxysilanes: Catalytic Production of Cross-Linkable Polyethylene and Elucidation of the Chain-Growth Mechanism. *J. Am. Chem. Soc.* **2017**, *139*, 16013–16022. [CrossRef] [PubMed]
43. O'Connor, K.S.; Lamb, J.R.; Vaidya, T.; Keresztes, I.; Klimovica, K.; LaPointe, A.M.; Daugulis, O.; Coates, G.W. Understanding the Insertion Pathways and Chain Walking Mechanisms of α-Diimine Nickel Catalysts for α-Olefin Polymerization: A ^{13}C NMR Spectroscopic Investigation. *Macromolecules* **2017**, *50*, 7010–7027. [CrossRef]
44. Kaiser, J.M.; Anderson, W.C., Jr.; Long, B.K. Photochemical regulation of a redox-active olefin polymerization catalyst: Controlling polyethylene microstructure with visible light. *Polym. Chem.* **2018**, *9*, 1567–1570. [CrossRef]
45. Gurinovich, N.S.; Petrovsky, S.K.; Saliy, I.V.; Saraev, V.V. Influence of a diimine ligand and an activator on the processes taking place in Brookhart-type nickel catalytic systems. *Res. Chem. Intermed.* **2018**, *44*, 1935–1944. [CrossRef]
46. Soshnikov, I.E.; Semikolenova, N.V.; Bryliakov, K.P.; Antonov, A.A.; Zakharov, V.A.; Talsi, E.P. NMR spectroscopic identification of Ni(II) species formed upon activation of (α-diimine)$NiBr_2$ polymerization catalysts with MAO and MMAO. *Dalton Trans.* **2018**, *47*, 4968–4974. [CrossRef]
47. Wang, B.; Daugulis, O.; Brookhart, M. Ethylene Polymerization with Ni(II) Diimine Complexes Generated from 8-Halo-1-naphthylamines: The Role of Equilibrating Syn/Anti Diastereomers in Determining Polymer Properties. *Organometallics* **2019**, *38*, 4658–4668. [CrossRef]
48. Soshnikov, I.E.; Semikolenova, N.V.; Bryliakov, K.P.; Antonov, A.A.; Sun, W.H.; Talsi, E.P. EPR spectroscopic study of Ni(I) species in the catalyst system for ethylene polymerization based on α-diimine Ni(II) complex activated by MMAO. *J. Organomet. Chem.* **2019**, *880*, 267–271. [CrossRef]
49. Chapleski, R.C., Jr.; Kern, J.L.; Anderson, W.C., Jr.; Long, B.K.; Roy, S. A mechanistic study of microstructure modulation in olefin polymerizations using a redox-active Ni(II) α-diimine catalyst. *Catal. Sci. Technol.* **2020**, *10*, 2029–2039. [CrossRef]
50. Tran, Q.H.; Wang, X.; Brookhart, M.; Daugulis, O. Cationic α-Diimine Nickel and Palladium Complexes Incorporating Phenanthrene Substituents: Highly Active Ethylene Polymerization Catalysts and Mechanistic Studies of syn/anti Isomerization. *Organometallics* **2020**, *39*, 4704–4716. [CrossRef]
51. Soshnikov, I.E.; Semikolenova, N.V.; Bryliakov, K.P.; Antonov, A.A.; Sun, W.H.; Talsi, E.P. Activation of an α-diimine Ni(II) precatalysts with $AlMe_3$ and $Al(^iBu)_3$: Catalytic and NMR and EPR spectroscopic studies. *Organometallics* **2020**, *39*, 3034–3040. [CrossRef]
52. Soshnikov, I.E.; Semikolenova, N.V.; Bryliakov, K.P.; Antonov, A.A.; Sun, W.H.; Talsi, E.P. The nature of nickel species formed upon the activation of α-diimine nickel(II) pre-catalyst with alkylaluminum sesquichlorides. *J. Organomet. Chem.* **2020**, *907*, 121063. [CrossRef]
53. Soshnikov, I.E.; Semikolenova, N.V.; Bryliakov, K.P.; Antonov, A.A.; Sun, W.H.; Talsi, E.P. Nature of Heterobinuclear Ni(I) Complexes Formed upon the Activation of the α-Diimine Complex $LNi^{II}Br_2$ with $AlMe_3$ and MMAO. *Organometallics* **2021**, *40*, 907–914. [CrossRef]
54. Soshnikov, I.E.; Semikolenova, N.V.; Bryliakov, K.P.; Talsi, E.P. α-Diimine Ni-Catalyzed Ethylene Polymerizations: On the Role of Nickel(I) Intermediates. *Catalysts* **2021**, *11*, 1386. [CrossRef]
55. Xu, S.; Chen, X.; Luo, G.; Gao, W. Nickel complexes based on BIAN ligands: Transformation and catalysis on ethylene polymerization. *Dalton Trans.* **2021**, *50*, 7356–7363. [CrossRef]
56. Soshnikov, I.E.; Semikolenova, N.V.; Bryliakov, K.P.; Antonov, A.A.; Talsi, E.P. Ni(I) Intermediates Formed upon Activation of a Ni(II) α-Diimine Ethylene Polymerization Precatalyst with AlR_3 (R = Me, Et, and ^iBu), AlR_2Cl (R = Me, Et), and MMAO: A Comparative Study. *Organometallics* **2022**, *41*, 1015–1024. [CrossRef]
57. Leung, D.H.; Ziller, J.W.; Guan, Z. Axial Donating Ligands: A New Strategy for Late Transition Metal Olefin Polymerization Catalysis. *J. Am. Chem. Soc.* **2008**, *130*, 7538–7539. [CrossRef]
58. Cotton, F.A.; Wilkinson, G.; Murillo, C.A.; Bochmann, M. *Advanced Inorganic Chemistry*, 6th ed.; Wiley: New York, NY, USA, 1999; pp. 840–842.

59. Soshnikov, I.E.; Semikolenova, N.V.; Zakharov, V.A.; Moller, H.M.; Olscher, F.; Osichow, A.; Gottker-Schnettmann, I.; Mecking, S.; Talsi, E.P.; Bryliakov, K.P. Formation and Evolution of Chain-Propagating Species Upon Ethylene Polymerization with Neutral Salicylaldiminato Nickel(II) Catalysts. *Chem. Eur. J.* **2013**, *19*, 11409–11417. [CrossRef] [PubMed]
60. Antonov, A.A.; Semikolenova, N.V.; Zakharov, V.A.; Zhang, W.; Wang, Y.; Sun, W.-H.; Talsi, E.P.; Bryliakov, K.P. Vinyl Polymerization of Norbornene on Nickel Complexes with Bis(imino)pyridine Ligands Containing Electron-Withdrawing Groups. *Organometallics* **2012**, *31*, 1143–1149. [CrossRef]
61. Antonov, A.A.; Samsonenko, D.G.; Talsi, E.P.; Bryliakov, K.P. Formation of Cationic Intermediates upon the Activation of Bis(imino)pyridine Nickel Catalysts. *Organometallics* **2013**, *32*, 2187–2191. [CrossRef]
62. NMR of Paramagnetic Molecules. *Principles and Applications*; La Mar, G.N., Horrocks, W.D.W., Jr., Holm, R.H., Eds.; John Wiley & Sons, Inc.: Hoboken, NJ, USA, 1973.
63. Krzystek, J.; Park, J.H.; Meisel, M.W.; Hitchman, M.A.; Stratemeier, H.; Brunel, L.C.; Telser, J. EPR Spectra from "EPR-Silent" Species: High-Frequency and High-Field EPR Spectroscopy of Pseudotetrahedral Complexes of Nickel(II). *Inorg. Chem.* **2002**, *41*, 4478–4487. [CrossRef] [PubMed]
64. Pappas, I.; Treacy, S.; Chirik, P.J. Alkene Hydrosilylation Using Tertiary Silanes with α-Diimine Nickel Catalysts. Redox-Active Ligands Promote a Distinct Mechanistic Pathway from Platinum Catalysts. *ACS Catal.* **2016**, *6*, 4105–4109. [CrossRef]
65. Gordon, A.J.; Ford, R.A. *The Chemist's Companion: A Handbook of Practical Data, Techniques, and References*, 1st ed.; Wiley-Interscience: New York, NY, USA, 1972.
66. Zhang, J.; Rahman, M.M.; Zhao, Q.; Feliciano, J.; Bisz, E.; Dziuk, B.; Lalancette, R.; Szostak, R.; Szostak, M. N-Heterocyclic Carbene Complexes of Nickel(II) from Caffeine and Theophylline: Sustainable Alternative to Imidazol-2-ylidenes. *Organometallics* **2022**, *41*, 1806–1815. [CrossRef] [PubMed]
67. Douthwaite, R.E.; Green, M.L.H.; Silcock, P.J. Nickel(II) cis- and trans-Dimethyl Complexes of Di-N-heterocyclic Carbenes. *Organometallics* **2001**, *20*, 2611–2615. [CrossRef]
68. Ottenbacher, R.V.; Bryliakova, A.A.; Shashkov, M.V.; Talsi, E.P.; Bryliakov, K.P. To Rebound or...Rebound? Evidence for the "Alternative Rebound" Mechanism in C–H Oxidations by the Systems Nonheme Mn Complex/H_2O_2/Carboxylic Acid. *ACS Catal.* **2021**, *11*, 5517–5524. [CrossRef]
69. Zima, A.M.; Lyakin, O.Y.; Bryliakova, A.A.; Babushkin, D.E.; Bryliakov, K.P.; Talsi, E.P. Reactivity vs. Selectivity of Biomimetic Catalyst Systems of the Fe(PDP) Family through the Nature and Spin State of the Active Iron-Oxygen Species. *Chem. Rec.* **2022**, *22*, e202100334. [CrossRef]
70. Zima, A.M.; Lyakin, O.Y.; Bryliakova, A.A.; Babushkin, D.E.; Bryliakov, K.P.; Talsi, E.P. Effect of Brønsted Acid on the Reactivity and Selectivity of the Oxoiron(V) Intermediates in C-H and C=C Oxidation Reactions. *Catalysts* **2022**, *12*, 949. [CrossRef]
71. Babushkin, D.E.; Semikolenova, N.V.; Zakharov, V.A.; Talsi, E.P. Mechanism of dimethylzirconocene activation with methylaluminoxane: NMR monitoring of intermediates at high Al/Zr ratios. *Macromol. Chem. Phys.* **2000**, *201*, 558–567. [CrossRef]
72. Sun, J.; Wang, F.; Li, W.; Chen, M. Ligand steric effects on alpha-diimine nickel catalyzed ethylene and 1-hexene polymerization. *RSC Adv.* **2017**, *7*, 55051–55059. [CrossRef]
73. Walters, W.D. Exchange Reaction of Biacetyl with Deuterium Oxide. *J. Am. Chem. Soc.* **1941**, *63*, 2850–2851. [CrossRef]
74. Grimme, S.; Antony, J.; Ehrlich, S.; Krieg, H. A consistent and accurate ab initio parameterization of density functional dispersion correction (DFT-D) for the 94 elements H-Pu. *J. Chem. Phys.* **2010**, *132*, 154104. [CrossRef]
75. Frisch, M.J.; Trucks, G.W.; Schlegel, H.B.; Scuseria, G.E.; Robb, M.A.; Cheeseman, J.R.; Scalmani, G.; Barone, V.; Petersson, G.A.; Nakatsuji, H.; et al. *Gaussian 16, Revision, C.01*; Gaussian, Inc.: Wallingford, CT, USA, 2019.
76. Weigend, F.; Ahlrichs, R. Balanced basis sets of split valence, triple zeta valence and quadruple zeta valence quality for H to Rn: Design and assessment of accuracy. *Phys. Chem. Chem. Phys.* **2005**, *7*, 3297–3305. [CrossRef] [PubMed]
77. Krishnan, R.; Binkley, J.S.; Seeger, R.; Pople, J.A. Self-consistent molecular orbital methods. XX. A basis set for correlated wave functions. *J. Chem. Phys.* **1980**, *72*, 650–654. [CrossRef]
78. Miertuš, S.; Scrocco, E.; Tomasi, J. Electrostatic interaction of a solute with a continuum. A direct utilization of ab initio molecular potentials for the prevision of solvent effects. *Chem. Phys.* **1981**, *55*, 117–129. [CrossRef]
79. Pascual-Ahuir, J.L.; Silla, E.; Tuñón, I. GEPOL: An improved description of molecular-surfaces. 3. A new algorithm for the computation of a solvent-excluding surface. *J. Comp. Chem.* **1994**, *15*, 1127–1138. [CrossRef]